Magnetoelastic standing waves induced in UO_2 by microsecond magnetic field pulses

Rico Schönemann[a,1], George Rodriguez[b], Dwight Rickel[a], Fedor Balakirev[a], Ross D. McDonald[a], Jordan A. Evans[a,c], Boris Maiorov[a], Charles Paillard[d,e,f], Laurent Bellaiche[e,f], Andreas V. Stier[a,g], Myron B. Salamon[a], Krzysztof Gofryk[c], and Marcelo Jaime[a,1]

[a]Materials Physics and Applications–National High Magnetic Field Laboratory, Pulse Field Facility, Los Alamos National Laboratory, Los Alamos, NM 87545; [b]Detonation Science and Technology, Los Alamos National Laboratory, Los Alamos, NM 87545; [c]Nuclear Fuels and Materials Division, Idaho National Laboratory, Idaho Falls, ID 83415; [d]Laboratoire Structures, Propriétés et Modélisation des Solides, UMR8580 Centrale Supélec/CNRS, Université Paris-Saclay, F-91190 Gif Sur Yvette, France; [e]Physics Department, University of Arkansas, Fayetteville, AR 72701; [f]Institute for Nanoscience and Engineering, University of Arkansas, Fayetteville, AR 72701; and [g]Walter Schottky Institut, Physik-Department, Technische Universität München, 85748 Garching, Germany

Edited by J. C. Davis, Department of Physics, University of Oxford, Oxford, United Kingdom; received June 7, 2021; accepted October 29, 2021

Magnetoelastic dilatometry of the piezomagnetic antiferromagnet UO_2 was performed via the fiber Bragg grating method in magnetic fields up to 150 T generated by a single-turn coil setup. We show that in microsecond timescales, pulsed-magnetic fields excite mechanical resonances at temperatures ranging from 10 to 300 K, in the paramagnetic as well as within the robust antiferromagnetic state of the material. These resonances, which are barely attenuated within the 100-μs observation window, are attributed to the strong magnetoelastic coupling in UO_2 combined with the high crystalline quality of the single crystal samples. They compare well with mechanical resonances obtained by a resonant ultrasound technique and superimpose on the known nonmonotonic magnetostriction background. A clear phase shift of π in the lattice oscillations is observed in the antiferromagnetic state when the magnetic field overcomes the piezomagnetic switch field $H_c = -18$ T. We present a theoretical argument that explains this unexpected behavior as a result of the reversal of the antiferromagnetic order parameter at H_c.

single-turn coils | piezomagnetism | mechanical resonances | canted antiferromagnetism

The antiferromagnetic (AFM) insulator uranium dioxide UO_2 has been the subject of extensive research during the last decades predominantly due to its widespread use as nuclear fuel in commercial power reactors (1). Besides efforts to understand the unusually poor thermal conductivity of UO_2, which impacts its performance as nuclear fuel (2), a recent magnetostriction study in pulsed magnetic fields up to 92 T uncovered linear magnetostriction in UO_2 (3), a hallmark of piezomagnetism.

Piezomagnetism is characterized by the induction of a magnetic polarization by application of mechanical strain, which, in the case of UO_2, is enabled by broken time-reversal symmetry in the 3-*k* AFM structure that emerges below $T_N = 30.8$ K (4–7) and is accompanied by a Jahn–Teller distortion of the oxygen cage (8–11). This also leads to a complex hysteretic magnetoelastic memory behavior where magnetic domain switching occurs at fields around ± 18 T at $T = 2.5$ K. Interestingly, the very large applied magnetic fields proved unable to suppress the AFM state that sets in at T_N (3). These earlier results provide direct evidence for the unusually high energy scale of spin-lattice interactions and call for further studies in higher magnetic fields.

Here we present axial magnetostriction data obtained in a UO_2 single crystal in magnetic fields to 150 T. These ultrahigh fields were produced by single-turn coil pulsed resistive magnets (12, 13) and applied along the [111] crystallographic axis at various temperatures between 10 K and room temperature. At all temperatures, we observe a dominant negative magnetostriction proportional to H^2 accompanied by unexpectedly strong oscillations that establish a mechanical resonance in the sample virtually instantly upon delivery of the 10^2 T/μs pulsed magnetic field rate of change. The oscillations are long-lasting due to very low losses and match mechanical resonances obtained with a resonant ultrasound spectroscopy (RUS) technique (14). Mechanical resonances were suggested to explain anomalies in magnetostriction measurements during single-turn pulses (15, 16); however, their potential to elucidate magnetic dynamics was not explored so far. When the sample is cooled below room temperature, the frequencies soften, consistent with observations in studies of the UO_2 elastic constant c_{44} as a function of temperature (17, 18).

In the AFM state, i.e., $T < 30.8$ K, the characteristic magnetic field sign switch in our single-turn coil magnet (a feature of destructive magnets) results in applied field values in excess of the UO_2 AFM domain switch field of $H_c \approx -18$ T. This field sign switch exposes yet another unexpected result, namely, a π (180°) phase shift in the magnetoelastic oscillations. We use a driven harmonic oscillator and an analytical model to shed light on the origin of the observed phase shift.

Results

Plots of the axial magnetostriction $\epsilon_a = \Delta l/l_0$, where $\Delta l/l_0$ is the change in the sample length normalized by its zero field value, vs. magnetic field at $T = 10$ K and $T = 70$ K are displayed in Fig. 1*C*. We observe an overall negative magnetostriction signal at high

Significance

UO_2 is of particular interest due to its use as a nuclear fuel, its unusually poor thermal conductivity, and its uniquely strong magnetoelastic properties characterized by a linear coupling between strain and magnetization. We clearly observe mechanical standing waves and elastic resonances in a single crystal, induced by microsecond magnetic field pulses. The phase and amplitude of the mechanical resonances are modulated by the piezomagnetic switching behavior, offering a sensitive probe for otherwise hard to detect magnetic dynamics in UO_2. We highlight the importance of magnetic domains in the attenuation of the mechanical resonances and the robustness of the antiferromagnetic state in UO_2 against externally applied magnetic fields to 150 T.

Author contributions: M.B.S., K.G., and M.J. designed research; G.R., D.R., F.B., R.D.M., J.A.E., B.M., A.V.S., K.G., and M.J. performed research; R.S., C.P., and L.B. contributed new reagents/analytic tools; R.S. and M.J. analyzed data; and R.S., C.P., M.B.S., K.G., and M.J. wrote the paper.

The authors declare no competing interest.

This article is a PNAS Direct Submission.

[1]To whom correspondence may be addressed. Email: rschoenemann@lanl.gov or mjaime@lanl.gov.

This article contains supporting information online at https://www.pnas.org/lookup/suppl/doi:10.1073/pnas.2110555118/-/DCSupplemental.

Published December 15, 2021.

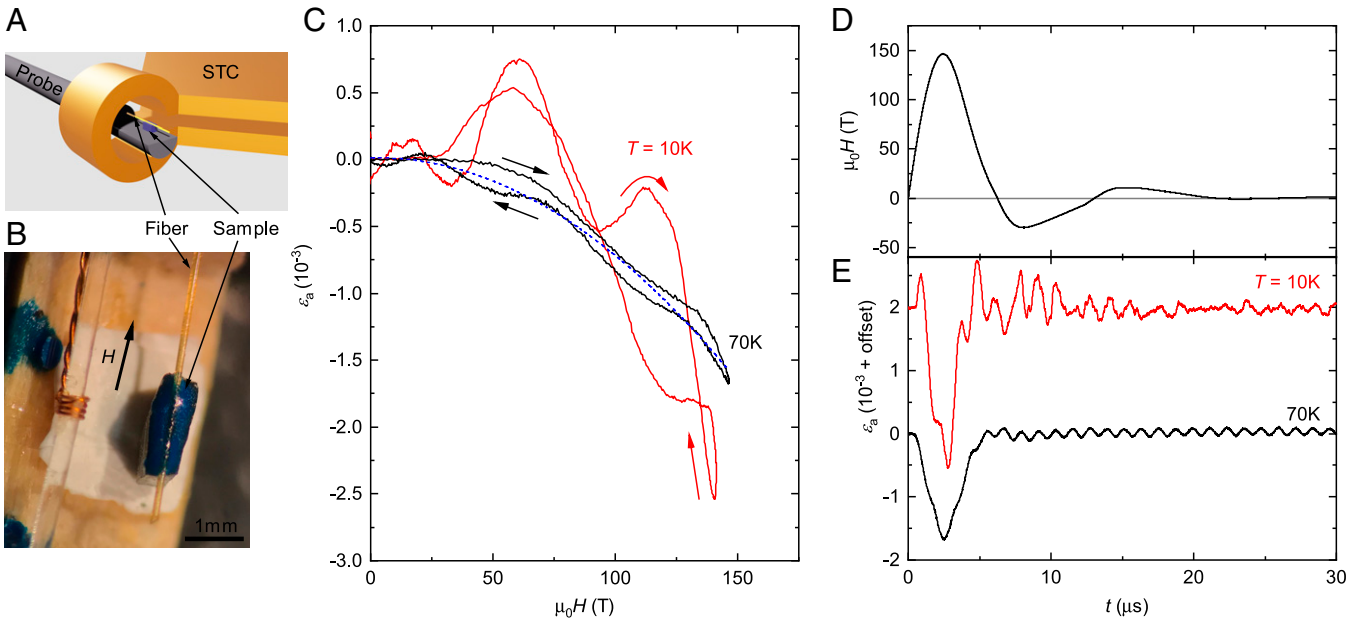

Fig. 1. Axial magnetostriction in UO_2. (*A*) Simplified depiction of the sample/fiber on the probe inside the single-turn coil (STC). (*B*) Picture of the UO_2 single crystal attached to the FBG-furnished fiber. Note that the sample is not physically attached to the sample holder, other than through the 125 μm optical fiber. A copper coil, located next to the sample, was used to measure the magnetic field. (*C*) Axial magnetostriction ϵ_a of a UO_2 single crystal along the [111] axis for $T = 10$ K (red line) and 70 K (black line). The dashed blue line is a second-order polynomial fit of the 70 K data representing the expected magnetostriction behavior. The arrows marking up and down sweep of the magnetic field. (*D*) Magnetic field vs. time of a typical single-turn coil field pulse. (*E*) ϵ_a as a function of time for pulses at 10 and 70 K. The spike in ϵ_a during the first few microseconds is caused by the magnetostriction of the sample (shown in *C*) due to the changing magnetic field during the field pulse, whereas the oscillatory part of the signal continues after the field decayed to zero.

fields as expected from previous results in pulsed magnetic fields to 92 T (3) with no indication of suppression of the robust AFM order nor any sign of saturation of the magnetostriction up to 146 T (details can be found in *SI Appendix*). However, the signal is highly hysteretic due to the large mechanical resonances that are superimposed on the magnetostriction signal. The magnetostriction signal itself roughly follows a second-order polynomial field dependence.

The field-induced mechanical resonances become clearer when ϵ_a is plotted as a function of time (Fig. 1*E*). Oscillations start with the onset of the field pulse and persist during the entire data acquisition period (100 μs at 300 K, 50 μs for lower temperatures). From fits between 300 and 40 K, we estimate the characteristic damping timescale of the mechanical resonance to be between 160 and 80 μs, respectively. The high quality of our UO_2 crystal is probably a key factor behind the low attenuation of the mechanical resonances observed in the experiment. This is validated by a large quality factor $Q = f/w$ found by RUS and ranging from 2,500 to 5,000. Here f is the frequency and w is the width of the resonance (fitted by a Lorentzian).

The onset of the mechanical resonances is approximately instantaneous, which indicates that they arise as a response to the magnetic field change and the strong magnetoelastic coupling. Hence, it does not appear that this mechanism is triggered by the shock wave generated by the disintegration of the single-turn coil which would need a few microseconds to reach the sample. Indeed, it appears as if the excitation that reaches the sample travels at the speed of propagating electromagnetic waves rather than the speed of sound. A similar experiment run with identical interrogation parameters and a bare fiber Bragg grating (FBG) sensor, i.e., with no sample attached to the fiber, yielded no detectable mechanical resonances.

In order to understand the origin of the observed mechanical resonances, we compare the typical field vs. time profile of a 146 T pulse performed in a single-turn coil (Fig. 2*A*) with a 60 T shot in a nondestructive short pulse magnet (Fig. 2*B*). The field generated by the short pulse magnet has a total duration of about 100 ms with a rise time of 10 ms. The single-turn coil, on the other hand, has a pulse duration on the order of 25 μs and a rise time of 2.5 μs (4,000× faster compared to the nondestructive magnet). Furthermore, the field switches sign several times, referred to as magnetic field recoil, displaying a significantly less attenuated behavior than the short pulse magnet. The relatively short timescales in the single-turn pulse result in a shift of the fast Fourier transform (FFT) of the field pulse toward higher frequencies up to several MHz, which is displayed in Fig. 2*C*. Thus, the spectral component around 800 kHz in the single-turn coil pulse is amplified by 60 dB and able to excite resonances with an amplitude of $\epsilon_a \approx 10^{-4}$ that one would not be able to resolve in an experiment involving a short pulse magnet, where the resonance amplitudes would be on the order of $\epsilon_a \approx 10^{-7}$. Therefore, if the system under study is magnetic, the field pulse of a single-turn coil itself can, by virtue of the strong magnetoelastic coupling present in UO_2 (17, 19, 20), excite mechanical resonances in the range of several hundred kHz. Note that mechanical resonances can also be studied in high static magnetic fields with contactless RUS techniques relying on magnetostrictive thin films (21, 22), but this technique is limited by strain lag across the interface between the film and sample.

The FFT of ϵ_a in UO_2 reveals three distinct frequencies labeled f_1, f_2, and f_3 for temperatures between 10 and 300 K, as shown in Fig. 3*B*. All modes display a softening as the temperature is lowered and a stiffening below T_N (Fig. 3*C*), in agreement with previous measurements of the elastic constants of UO_2 which show a similar behavior (17). Three independent elastic constants c_{11}, c_{12}, and c_{44} exist for a lattice with cubic symmetry. The distinct temperature dependence of all three mechanical resonance frequencies f_{1-3} is dominated by c_{44} due to the large change of c_{44} as a function of temperature as reported in refs. 17, 18. We confirmed that the mechanical resonances are similar to those observed by resonant ultrasound at 300 K, as shown in Fig. 3*D*. The RUS measurements reveal a rich spectrum of

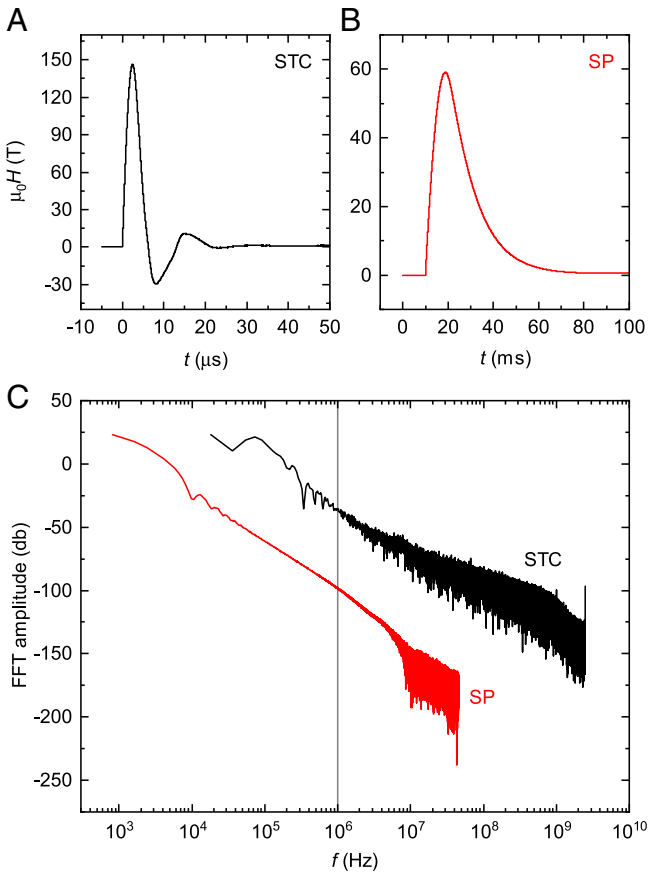

Fig. 2. Magnetic field profiles. (*A*) Magnetic field vs. time of a 146 T pulse in a single-turn coil and (*B*) a 60 T pulse in a nondestructive short pulse magnet. (*C*) Fourier transformations of the field vs. time curves shown in (A) and (*B*). The field profiles and FFT's of the short pulse magnet and single-turn pulses are depicted by red and black lines, respectively.

sharp resonances in the frequency range up to 1 MHz. When the crystal is attached to the fiber a broadening of resonance peaks, accompanied by a decrease in amplitude, is observed. This increased damping is a product of a larger system consisting of the crystal, glue, and fiber. Nevertheless, the overall range of mechanical resonance frequencies observed in the magnetostriction measurements is comparable with RUS spectra. In the FBG measurements we observe three distinct frequencies. The additional mechanical resonance frequencies present in the RUS spectra are potential resonances that either are completely damped by the attached fiber and encapsulant or only have a small compressive component parallel to the fiber since the FBG method is less sensitive to sheer strain. Note that the RUS measurements on the bare UO_2 crystal were performed on a $\approx$ 2 mm longer sample than the FBG and RUS measurements with the optical fiber attached. The change of the sample geometry also affects the mechanical resonance frequencies.

Upon cooling the sample below the AFM transition we observe a substantial change in the mechanical resonances when compared to temperatures above T_N:

1) In the data recorded at 10 K, within the AFM ordered phase, the resonances appear to be significantly damped after $t \approx 7$ μs; in particular, the FFT amplitude of $f_3 = 800$ kHz is suppressed when compared to f_1 and f_2, in contrast to the Fourier transforms of the datasets above T_N where f_3 is clearly the dominant resonance (Fig. 3*B*). The attenuation effect becomes more apparent when band pass filters are applied to the experimental data, isolating the individual resonances and removing the magnetostriction background (Fig. 4 *A*, *B*, and *D*). We show that when compared to f_3, the amplitude of lower resonances f_2 and f_3 does not display a drastic change for $t > 7$ μs.
2) A π phase shift can be observed in the mechanical resonances at $t \approx 7$ μs, which is accompanied by the observed attenuation effect. One can clearly identify the π phase shift after a 700 to 1,200 kHz band pass filter was applied to the experimental data (Fig. 4*D*). The pronounced beating pattern in f_3 (Fig. 4 *C* and *D*) is an artifact from the band pass filter and depends on the choice of the cutoff frequencies, whereas the phase shift is a robust physical feature. Interestingly, only f_3 shows the phase shift, and both lower resonances f_1 and f_2 seem not to be affected and follow a single sinusoidal function as shown in Fig. 4*D*.

The phase shift around $t \approx 7$ μs coincides with a magnetic field value of approximately -18 T close to the field value where an abrupt sign change of the AFM ordering vector L_0 (as defined in ref. 23) leads to a jump in the lattice distortion and the characteristic piezomagnetic butterfly that was reported in ref. 3.

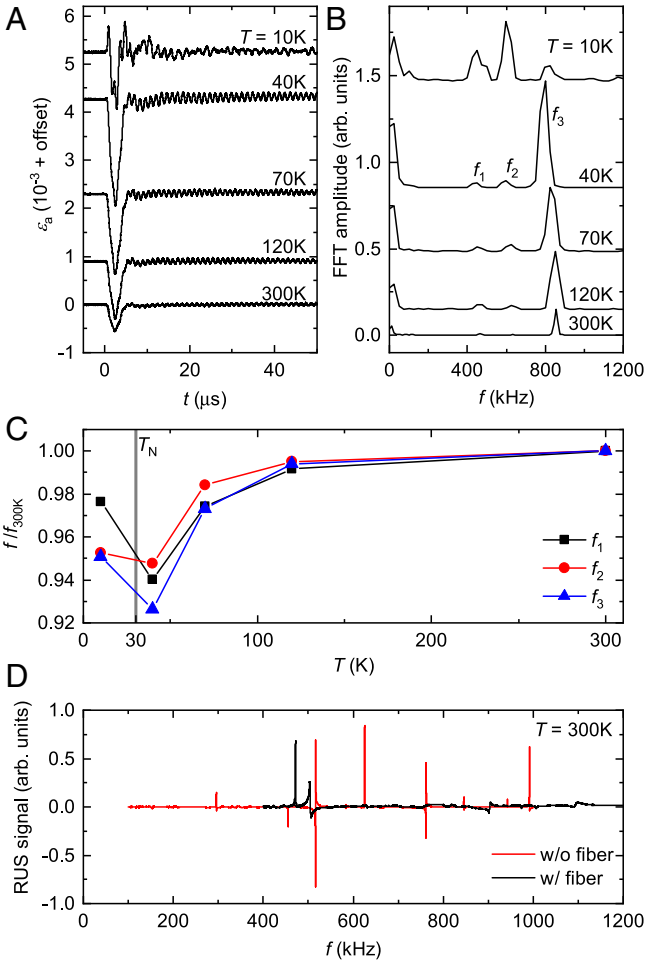

Fig. 3. Mechanical resonances in UO_2. (*A*) Axial magnetostriction vs. time for different temperatures between 10 and 300 K. Curves are shifted for clarity. (*B*) Fourier transforms of ϵ_a showing three dominant frequencies labeled as f_1, f_2, and f_3. The low-frequency peaks below 200 kHz originate from the background magnetostriction. (*C*) Normalized temperature dependence of $f_{1,2,3}$. (*D*) RUS spectra at $T = 300$ K. The RUS spectra of the bare sample (black line) and the sample with the attached optical fiber (red line) were recorded along the [111] axis.

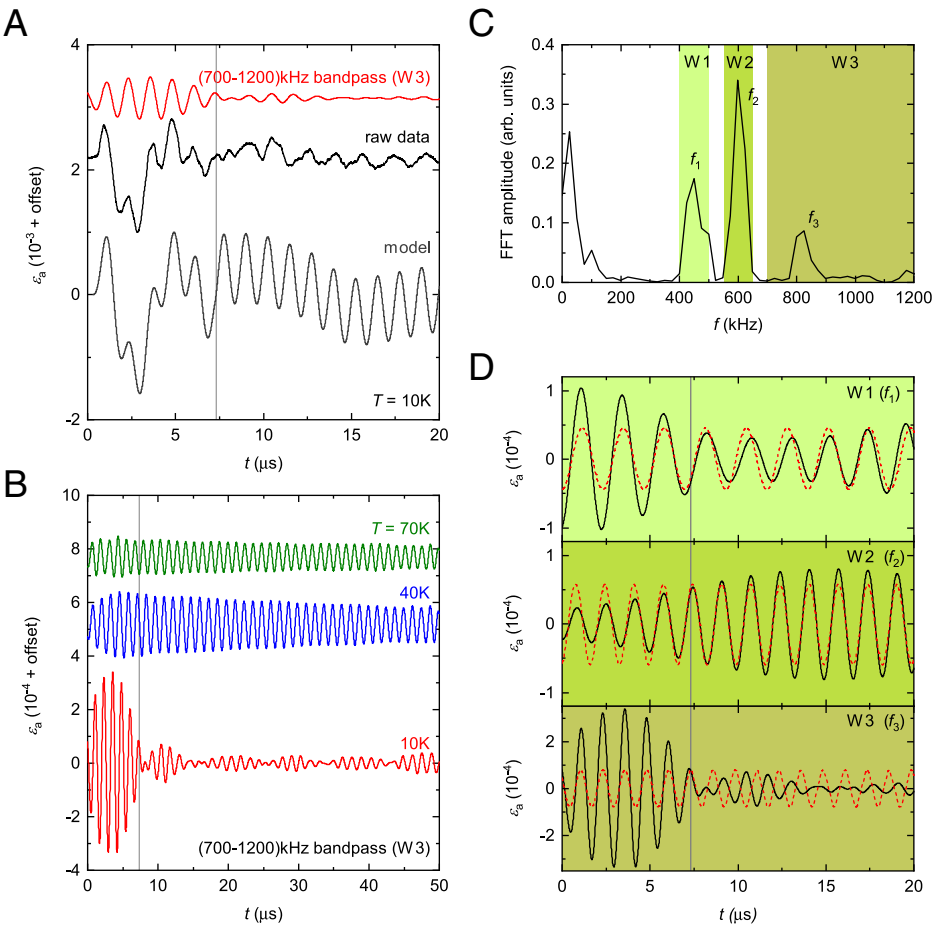

Fig. 4. Mechanical resonances in the AFM state. (*A*) ϵ_a vs. time at 10 K with a peak field of 126 T before (black line) and after (red line) the 700 to 1,200 kHz band pass filter was applied. The experimental data are compared to a driven harmonic oscillator model with a characteristic frequency of 800 kHz matching the dominant oscillations seen during the field pulse in the magnetostriction signal (gray curve). The experimental data and the model show a π phase shift around 7.3 μs marked by the gray vertical line. (*B*) Magnetoelastic oscillations at 10, 40, and 70 K after application of a 700 to 1,200 kHz band pass filter to the experimental data. Curves are shifted for clarity. (*C*) FFT of ϵ_a at $T = 10$ K. The windows of the band pass filter (W1, W2, and W3) are highlighted in different colors. (*D*) FFT filtered curves (black lines) for each window compared with sinusoidal functions indicated as red dashed lines.

This effect is illustrated in Fig. 5 with the piezomagnetic butterfly shown in Fig. 5, *Inset*. The phase shift can also be observed in field pulses with a peak field below 30 T (*SI Appendix*). The origin of the phase shift can be found in the sudden reversal of L_0 (red) to the $-L_0$ (blue) as we demonstrate in the following.

Following Bar'yakhtar et al. (23), we denote as $\boldsymbol{L}_1$, $\boldsymbol{L}_2$ and $\boldsymbol{L}_3$ the different AFM vectors that describe the 3-*k* order in UO_2, and $\boldsymbol{M}$ the average magnetization. The magnetic unit cell below the AFM transition is made of four formula units, each formula unit carrying a magnetic moment $\boldsymbol{S}_1$, $\boldsymbol{S}_2$, $\boldsymbol{S}_3$, and $\boldsymbol{S}_4$. The above AFM vectors and magnetization can be expressed, in terms of the individual magnetic moments, as

$$\begin{aligned}\boldsymbol{M} &= \boldsymbol{S}_1 + \boldsymbol{S}_2 + \boldsymbol{S}_3 + \boldsymbol{S}_4,\\ \boldsymbol{L}_1 &= \boldsymbol{S}_1 + \boldsymbol{S}_2 - \boldsymbol{S}_3 - \boldsymbol{S}_4,\\ \boldsymbol{L}_2 &= \boldsymbol{S}_1 - \boldsymbol{S}_2 + \boldsymbol{S}_3 - \boldsymbol{S}_4,\\ \boldsymbol{L}_3 &= \boldsymbol{S}_1 - \boldsymbol{S}_2 - \boldsymbol{S}_3 + \boldsymbol{S}_4.\end{aligned}$$

In the Landau approach, the thermodynamic potential must be able to describe both the paramagnetic and AFM phases. This is achieved by performing a polynomial expansion of the free energy whose terms respect the symmetry of the highest symmetry phase (24). Such terms have already been worked out in ref. 23. The Hamiltonian of the system can thus be written as

$$\hat{H} = \int d^3\boldsymbol{r}\hat{\mathcal{H}}(\boldsymbol{r}), \qquad [1]$$

where $\hat{\mathcal{H}}$ can be found in *SI Appendix*. Since we are primarily interested in explaining the properties of the mechanical resonances and the π phase shift in response to an applied pulsed magnetic field, we make the simplifying following assumption: the magnetic response of the sample is primarily determined by the external magnetic field, and elastic vibrations do not affect it significantly. As a result, we write each magnetic quantity under the form $\boldsymbol{\mu} = \boldsymbol{\mu}_{eq} + \delta\boldsymbol{\mu}$ (with $\mu = L_1, L_2, L_3, M$). $\boldsymbol{\mu}_{eq}$ represents an equilibrium value, and $\delta\boldsymbol{\mu}$ represents the deviation away from that value, i.e., the response to the magnetic pulse.

We then write the mechanical equations of motion, from which we retain $\rho\ddot{u}_x$,

$$\rho\ddot{u}_x = \frac{\partial}{\partial x}\left(\frac{\partial\hat{\mathcal{H}}}{\partial\eta_1}\right) + \frac{\partial}{\partial y}\left(\frac{\partial\hat{\mathcal{H}}}{\partial\eta_6}\right) + \frac{\partial}{\partial z}\left(\frac{\partial\hat{\mathcal{H}}}{\partial\eta_5}\right). \qquad [2]$$

In the mechanical equations, ρ is the volumic mass, and u_α is the displacement field in direction α. Since the derivations are lengthy, we will focus on the component u_x of the displacement field which, after replacing with the Hamiltonian expression (*SI Appendix*) and assuming, as demonstrated in ref. 23, that at equilibrium, $L_{1x}^{eq} = L_0$, $L_{2y}^{eq} = L_0$, and $L_{3z}^{eq} = L_0$, we write

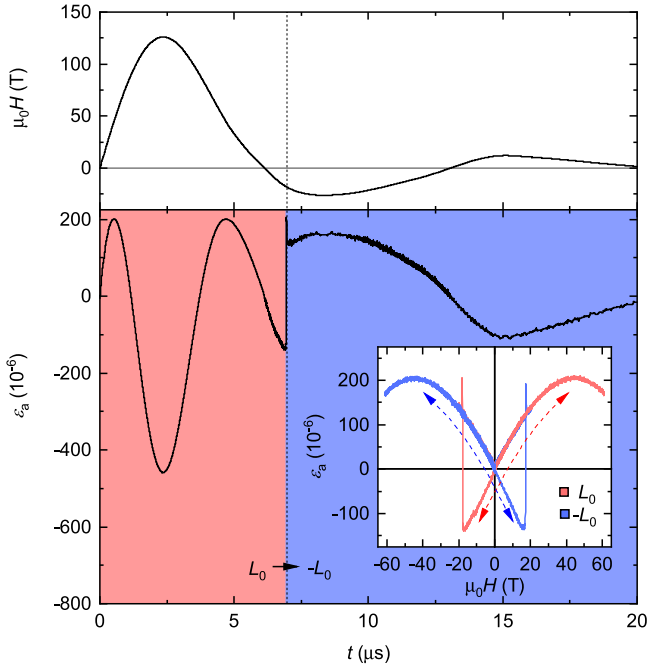

Fig. 5. Piezomagnetic switching in UO_2. (*Upper*) Magnetic field and (*Lower*) axial magnetostriction of UO_2 as a function of time. The magnetostriction data were mapped and extrapolated onto the single-turn field profile using previously published pulse field data shown in *Inset* (reprinted from ref. 3, which is licensed under CC BY 4.0; https://creativecommons.org/licenses/by/4.0/). The vertical line at $t \approx 7$ μs separates the two states with positive (red) and negative (blue) AFM ordering vector L_0 by reaching the switching field of ≈ -18 T in this case.

$L_{1x} = L_0 + \delta L_{1x}$, $L_{1y} = \delta L_{1y}$, $L_{1z} = \delta L_{1z}$, etc. Similarly, ref. 3 shows that no magnetization seems to exist in the AFM phase, so we write $M_x = \delta M_x$, etc. We also recall that $\eta_1 = \frac{\partial u_x}{\partial x}$, $\eta_5 = \frac{\partial u_x}{\partial z} + \frac{\partial u_z}{\partial x}$; the equation can now be written, for linear terms, as

$$\begin{aligned}\rho\ddot{u}_x \approx\ & c_{11}\frac{\partial^2 u_x}{\partial x^2} + c_{12}\left(\frac{\partial^2 u_y}{\partial x\partial y} + \frac{\partial^2 u_z}{\partial x\partial z}\right)\\ &+ c_{44}\left(\frac{\partial^2 u_x}{\partial y^2} + \frac{\partial^2 u_y}{\partial y\partial x} + \frac{\partial^2 u_z}{\partial z\partial x} + \frac{\partial^2 u_x}{\partial z^2}\right)\\ &+ L_0(\lambda_1 + \lambda_1')\frac{\partial\delta L_{1x}}{\partial x} + \lambda_1' L_0\left(\frac{\partial\delta L_{2y}}{\partial x} + \frac{\partial\delta L_{3z}}{\partial x}\right)\\ &+ \frac{\lambda}{2}L_0\left(\frac{\partial\delta L_{1y}}{\partial y} + \frac{\partial\delta L_{2x}}{\partial y} + \frac{\partial\delta L_{1z}}{\partial z} + \frac{\partial\delta L_{3x}}{\partial z}\right). \qquad \textbf{[3]}\end{aligned}$$

In Eq. **3**, the terms proportional to λ_1, λ_1', and λ relate the linear change of shape of an AFM uniform domain with respect to AFM excitation.

If we perform a Fourier transform, $u_x = \int \frac{d\boldsymbol{q}}{2\pi}\int \frac{d\omega}{2\pi} u_x(\boldsymbol{q},\omega)\, e^{i(\boldsymbol{q}.\boldsymbol{r}-\omega t)}$, etc., yielding

$$\begin{aligned}\left(c_{11}q_x^2 + c_{44}\left[q_y^2 + q_z^2\right] - \rho\omega^2\right)u_x(\boldsymbol{q},\omega) =\ & \\ -(c_{44}+c_{12})q_x\left[q_y u_y(\boldsymbol{q},\omega) + q_z u_z(\boldsymbol{q},\omega)\right]\ & \\ + iq_x L_0(\lambda_1+\lambda_1')\delta L_{1x}(\boldsymbol{q},\omega)\ & \\ + iq_x L_0\lambda_1'\left(\delta L_{2y}(\boldsymbol{q},\omega) + \delta L_{3z}(\boldsymbol{q},\omega)\right)\ & \\ + \frac{\lambda}{2}L_0 q_y\left[\delta L_{1y}(\boldsymbol{q},\omega) + \delta L_{2x}(\boldsymbol{q},\omega)\right]\ & \\ + \frac{\lambda}{2}L_0 q_z\left[\delta L_{1z}(\boldsymbol{q},\omega) + \delta L_{3x}(\boldsymbol{q},\omega)\right]. \qquad \textbf{[4]}\end{aligned}$$

We now have sets of coupled harmonic oscillators which are driven by a force which is proportional to L_0 (a cyclic permutation $x \to y \to z$ allows us to get the equations for the other components). In other words, given a proper change of basis, we can diagonalize this set of equations and write the displacement fields dynamical equations under the form

$$(\omega_0(\boldsymbol{q})^2 - \omega^2)u_1(\boldsymbol{q},\omega) = F_1(\boldsymbol{q},\omega),$$

with $F_1(\boldsymbol{q},\omega)$ being the force driving the oscillation of u_1 at pulsation ω with wave vector $\boldsymbol{q}$. This has an obvious solution, which is

$$u_1(\boldsymbol{q},\omega) = \frac{F_1(\boldsymbol{q},\omega)}{\omega_0(\boldsymbol{q})^2 - \omega^2}.$$

We note that F_1 is proportional to L_0, the AFM order parameter. It is then clear that upon reversal of the AFM order, $L_0 \longrightarrow -L_0$, the force applied on the set of harmonic oscillators reverses sign, i.e., $F_1 \to -F_1 = e^{i\pi}F_1$, and thus, a π phase shift must be experienced in the elastic oscillatory response of the sample long enough after the pulse. Hence, sufficient switching of the AFM order is likely the cause of the phase shift observed in the mechanical resonances. It is to be noted that the main energy couplings responsible for such an effect are quadratic in the AFM vectors and linear in strain; in other words, they are typical (antiferro)magnetostriction terms. We note that some of those energy couplings are the same ones from which piezomagnetism arises (see equations 31 and 32 from ref. 23).

Therefore, by assuming that the force driving the oscillations is proportional to the systems strain (shown in Fig. 5) and fixing the frequency at 800 kHz, we are able to model the experimental data with a simple driven harmonic oscillator. As depicted in Fig. 4*A*, this harmonic oscillator model reproduces the magnetostriction background as well as the π phase shift in the 800 kHz oscillations. The attenuation observed in the oscillations after the switching of L_0 is not captured by the model. We return to this point with more detail in the *Discussion*.

Discussion

A recent X-ray study on UO_2 single crystals evidences the presence of AFM domains and subsequently the coexistence of AFM phases L_0 and $-L_0$ connected by time-reversal even in magnetic fields beyond the piezomagnetic switching field (25). This is also supported by magnetostriction measurements (3), which show that the first pulse taken below T_N always has a smaller magnetostriction slope for fields below the switching field. This could be caused by the coexistence of all possible domains, with some contracting and some expanding as the field increases. In our measurements we observe a large attenuation effect around the switching field, but oscillations seem not to be further damped afterward. Therefore, the attenuation of f_3 appears to be caused by the coupling of the mechanical resonances to critical spin fluctuations and/or domain movement close to the piezomagnetic switching field which can lead to a significant attenuation of the mechanical resonances similar to the dramatically increased ultrasonic attenuation that was observed in UO_2 in the vicinity of the AFM phase transition (17). The mechanical resonances f_1 and f_2 might have a predominantly transversal character which would explain the smaller amplitude and the absence of attenuation below T_N since the longitudinal or compressive modes are expected to be more affected by spin fluctuations (26). For future experiments we plan to perform magnetocaloric measurements to detect possible heating effects at the switching field caused by dissipative processes like domain movement.

Another interesting point is that the π phase shift only occurs in f_3. The effect is completely absent in f_2 and much less clear in f_1 which is only slightly out of phase when compared to the single sinusoidal function in the time interval between 0 and 20 μs (Fig. 4*D*). As of now we do not have a conclusive argument on why the phase shift is only visible in f_3. Depending on the involved AFM excitations and the anisotropy of the magnetoelastic

couplings, longitudinal and transversal mechanical resonances can display different phase shifts. A possible way to test this in future experiments is to use a birefringent FBG which can yield an orthogonal biaxial strain response along two directions with polarization-based probing techniques.

Persistent resonances are also present in fast pulses of 20 T and could potentially be exploited as a novel class of magnetic field–driven mechanical resonator which, given the extraordinary resilience of UO_2 against corrosion or radiation, could be suitable for harsh environments.

We demonstrate that mechanical resonances can be a useful tool to detect otherwise-elusive AFM domain flips and possibly also other types of crystallographic domain dynamics (e.g., in liquid crystals). On the other hand, our results indicate that mechanical resonances can also cause issues in experiments where they are unwanted. A mitigation strategy in experiments where excessive noise is prevalent could consist of clamping the sample as well as conducting runs with different sample and/or sample-holder geometries and dimensions to minimize mechanical resonances triggered by the magnetic field. This phenomenon is reminiscent of wire motion resonances in electrical transport experiments performed in short pulse magnets, which can be quite detrimental to the data quality and whose effects are minimized by fixing the wires and in this way effectively shifting their resonances to frequencies outside of the experimental range of interest.

Conclusions

We measured the lattice dilation along [111] up to 150 T in UO_2, in the AFM as well as in the paramagnetic states. Surprisingly, the AFM state is robust against a field of $146\,\mathrm{T}$ at $10\,\mathrm{K}$, energy-wise $\sim 5\times$ stronger than $T_\mathrm{N} = 30.8\,\mathrm{K}$ (if $g = 2$). Our results provide a test of the magnetoelastic coupling in UO_2 underscoring the large energy scale of electronic correlations in UO_2. We show that mechanical resonances can be induced virtually instantaneously via the magnetoelastic coupling in UO_2 by μs field pulses generated with the single-turn coil technique, making this material an interesting candidate for magnetoelastic transducers. We demonstrate in our theory modeling that the reversal of the AFM order, $L_0 \longrightarrow -L_0$, due to the piezomagnetic switching in UO_2 leads to a π phase shift in the standing waves and report a distinct mode dependent attenuation of the mechanical resonances. Our findings present a way to study magnetic dynamics in high magnetic fields and could have an impact on the interpretation of past and future data collected in experiments involving semidestructive pulsed magnetic fields as well practical implications, e.g., as a way to trigger resonators at faster speeds.

Materials and Methods

Fiber Bragg Grating Dilatometry. The magnetostriction signal of UO_2 was measured with a 100 MHz coherent pulse fiber Bragg interrogation method. The setup is driven by a modelocked pulsed 90 fs Er laser with a 100 MHz repetition rate and allows interrogation speed on the 10 ns scale. This method offers a faster readout rate than traditional FBG interrogation systems which operate in the range of several kHz (27). The UO_2 single crystal was attached to the optical fiber using an epoxy encapsulant with the crystallographic [111] axis aligned parallel to the fiber and the magnetic field (Fig. 1 *A* and *B*). The [111] axis is the easy magnetic axis for UO_2. Magnetostriction measurements at low temperatures ($T < 30$ K) along other directions were attempted multiple times, which resulted in the sample detaching from the optical fiber due to the large torque caused by the materials strong magnetic anisotropy in the AFM state. Details about the FBG setup can be found in ref. 15. During the field pulse, the induced voltage in a small copper coil, located in close proximity to the sample (Fig. 1*B*), was used to measure the magnetic field.

Single-Turn Coil Setup. The magnetic field was generated with a semi-destructive capacitor-driven single-turn coil magnet system at the National High Magnetic Field Laboratory (NHMFL)'s pulse field facility at Los Alamos National Laboratory (LANL). The system is designed for fields up to 300 T with a rise time of approximately 2.5 μs. Note that for magnetic fields in the region of 200 T and above, damage to the cryostat and sample becomes increasingly likely. Therefore, magnetic fields were limited to ≈ 150 T in this study, with a peak rate of change in the order of $10^2\,\mathrm{T}/\mu\mathrm{s}$. Further details about the single-turn coil setup are presented in refs. 12, 13. Optical measurement techniques, like the FBG method used here, are in general advantageous in single-turn experiments when compared to, e.g., electrical capacitance–based dilatometry measurements predominantly due to optical fibers being impervious to the large induced voltages generated inside even small metallic loops caused by the large dB/dt, as well as the associated electromagnetic interference.

RUS. The measurement of the natural mechanical resonances of elastic vibration where several normal modes of the sample are determined is obtained with a set of piezoelectric transducers using a technique known as RUS. Here one transducer serves as source of the tunable sinusoidal wave of frequency *f*, and the other serves as detector at the synchronous frequency of the sample's response. The electronics and room temperature apparatus are described in detail by Balakirev et al. (14). In our case, the transducer had an $Al_2\,O_3$ hemisphere that allows precise and reproducible point contact on desired positions of the crystal (28). As a frequency scan is performed, a resonance peak is observed at each of the normal modes. We performed resonant mode measurements on UO_2 single crystals alone as well with the 125 μm optical fiber attached.

Data Availability. Text documents and data have been deposited in Open Science Framework (DOI: 10.17605/OSF.IO/KCA7Y).

ACKNOWLEDGMENTS. We thank C. Mielke for single-turn coil magnet operation support and discussions. A portion of this work was performed at the National High Magnetic Field Laboratory, which is supported by the NSF Cooperative Agreement DMR-1644779 and the state of Florida. R.S. acknowledges funding through the Laboratory Directed Research and Development program of LANL and the G. T. Seaborg Institute under Project 20210527CR and the NHMFL User Collaboration Grants Program. C.P. and L.B. acknowledge the Army Research Office (ARO) Grant No. W911NF-21-1-0113 and the Vannevar Bush Faculty Fellowship (VBFF) Grant No. N00014-20-1-2834 from the Department of Defense. K.G. acknowledges support from the US Department of Energy (DOE) Early Career Research Program and US DOE Basic Energy Science (BES) Energy Frontier Research Center "Thermal Energy Transport under Irradiation." M.J. acknowledges support from the US DOE BES program through the project "Science at 100T" at LANL. M.J. and G.R. acknowledge support from the LANL Institute for Materials Science.

1. L. C. Wang, M. H. Kaye, "Oxide power reactor fuels" in *Advances in Nuclear Fuel Chemistry*, M. Piro, Ed. (Elsevier, 2020), pp. 185–213.
2. K. Gofryk *et al.*, Anisotropic thermal conductivity in uranium dioxide. *Nat. Commun.* **5**, 4551 (2014).
3. M. Jaime *et al.*, Piezomagnetism and magnetoelastic memory in uranium dioxide. *Nat. Commun.* **8**, 99 (2017).
4. P. Burlet *et al.*, Neutron diffraction on actinides. *J. Less Common Met.* **121**, 121–139 (1986).
5. R. Caciuffo *et al.*, Magnetic excitations and dynamical Jahn-Teller distortions in UO_2. *Phys. Rev. B Condens. Matter Mater. Phys.* **59**, 13892–13900 (Year1999).
6. E. Blackburn *et al.*, Spherical neutron spin polarimetry of anisotropic magnetic fluctuations in UO_2. *Phys. Rev. B Condens. Matter Mater. Phys.* **72**, 184411 (2005).
7. R. Caciuffo *et al.*, Anisotropic magnetic fluctuations in 3-k antiferromagnets. *J. Magn. Magn. Mater.* **310**, 1698–1702 (2007).
8. P. Giannozzi, P. Erdös, Theoretical analysis of the 3-k magnetic structure and distortion of uranium dioxide. *J. Magn. Magn. Mater.* **67**, 75–87 (1987).
9. K. Ikushima *et al.*, First-order phase transition in UO_2: ^{235}U and ^{17}O NMR study. *Phys. Rev. B Condens. Matter Mater. Phys.* **63**, 104404 (2001).
10. P. Santini *et al.*, Multipolar interactions in f-electron systems: The paradigm of actinide dioxides. *Rev. Mod. Phys.* **81**, 807–863 (2009).
11. R. Caciuffo *et al.*, Multipolar, magnetic, and vibrational lattice dynamics in the low-temperature phase of uranium dioxide. *Phys. Rev. B Condens. Matter Mater. Phys.* **84**, 104409 (2011).
12. C. H. Mielke, R. D. McDonald, "Single Turn Multi-Megagauss System at the NHMFL-LOS Alamos to study plutonium" in *2006 IEEE International Conference on Magagauss Magnetic Field Generation and Related Topics*, G. F. Kiuttu, P. J. Turchi, R. E. Reinovsky, Eds. (IEEE, Santa Fe, NM), pp. 227–231 (2006).
13. C. H. Mielke, B. M. Novac, Experimental and numerical studies of megagauss magnetic-field generation at LANL-NHMFL. *IEEE Trans. Plasma Sci.* **38**, 1739–1749 (2010).
14. F. F. Balakirev, S. M. Ennaceur, R. J. Migliori, B. Maiorov, A. Migliori, Resonant ultrasound spectroscopy: The essential toolbox. *Rev. Sci. Instrum.* **90**, 121401 (2019).
15. G. Rodriguez *et al.*, Coherent pulse interrogation system for fiber Bragg grating sensing of strain and pressure in dynamic extremes of materials. *Opt. Express* **23**, 14219–14233 (2015).
16. A. Ikeda *et al.*, High-speed 100 MHz strain monitor using fiber Bragg grating and optical filter for magnetostriction measurements under ultrahigh magnetic fields. *Rev. Sci. Instrum.* **88**, 083906 (2017).

17. O. G. Brandt, C. T. Walker, Temperature dependence of elastic constants and thermal expansion for UO_2. *Phys. Rev. Lett.* **18**, 11–13 (1967).
18. O. G. Brandt, C. T. Walker, Ultrasonic attenuation and elastic constants for uranium dioxide. *Phys. Rev.* **170**, 528–541 (1968).
19. G. Dolling, R. A. Cowley, A. D. B. Woods, The crystal dynamics of uranium dioxide. *Can. J. Phys.* **43**, 1397–1413 (1965).
20. G. Dolling, R. A. Cowley, Observation of magnon-phonon interaction at short wavelengths. *Phys. Rev. Lett.* **16**, 683–685 (1966).
21. V. Kuokkala, R. B. Schwarz, The use of magnetostrictive film transducers in the measurement of elastic moduli and ultrasonic attenuation of solids. *Rev. Sci. Instrum.* **63**, 3136–3142 (1992).
22. R. Schwarz, J. Vuorinen, Resonant ultrasound spectroscopy: Applications, current status and limitations. *J. Alloys Compd.* **310**, 243–250 (2000).
23. V. G. Bar'yakhtar, I. M. Vitebskii, D. A. Yablonskii, Magnetoelastic effects in non-collinear antiferromagnets. *Sov. Phys. JETP* **62**, 108 (1985).
24. J. C. Tolédano, P. Tolédano, *The Landau Theory of Phase Transitions* (World Scientific, 1987).
25. D. J. Antonio *et al.*, Piezomagnetic switching and complex phase equilibria in uranium dioxide. *Commun. Mater.* **2**, 17 (2021).
26. Y. Itoh, Ultrasonic attenuation in the simple cubic antiferromagnet near the néel temperature. *J. Phys. Soc. Jpn.* **38**, 336–344 (1975).
27. M. Jaime *et al.*, Fiber Bragg grating dilatometry in extreme magnetic field and cryogenic conditions. *Sensors (Basel)* **17**, 2572 (2017).
28. J. A. Evans *et al.*, Determining elastic anisotropy of textured polycrystals using resonant ultrasound spectroscopy. *J. Mater. Sci.* **56**, 10053–10073 (2021).